PAPER

Interactions of a lytic peptide with supported lipid bilayers investigated by time-resolved evanescent wave-induced fluorescence spectroscopy

IOP Publishing Methods Appl. Fluoresc. 4 (2016) 044001 doi:10.1088/2050-6120/4/4/044001

Methods and Applications in Fluorescence

PAPER

RECEIVED
14 June 2016

ACCEPTED FOR PUBLICATION
7 September 2016

PUBLISHED
28 September 2016

Interactions of a lytic peptide with supported lipid bilayers investigated by time-resolved evanescent wave-induced fluorescence spectroscopy

Andrew C Rapson[1], Michelle L Gee[1], Andrew H A Clayton[2] and Trevor A Smith[1]

[1] School of Chemistry, University of Melbourne, 3010 Victoria, Australia
[2] Centre for Micro-Photonics, Swinburne University of Technology, Hawthorn 3122, Australia

E-mail: trevoras@unimelb.edu.au and aclayton@swin.edu.au

Keywords: evanescent wave spectroscopy, melittin, antimicrobial peptide

Abstract

We report investigations, using time-resolved and polarised evanescent wave-induced fluorescence methods, into the location, orientation and mobility of a fluorescently labelled form of the antimicrobial peptide, melittin, when it interacts with vesicles and supported lipid bilayers (SLBs). This melittin analogue, termed MK14-A430, was found to penetrate the lipid headgroup structure in pure, ordered-phase DPPC membranes but was located near the headgroup-water region when cholesterol was included. MK14-A430 formed lytic pores in SLBs, and an increase in pore formation with incubation time was observed through an increase in polarity and mobility of the probe. When associated with the Cholesterol-containing SLB, the probe displayed polarity and mobility that indicated a population distributed near the lipid headgroup-water interface with MK14-A430 arranged predominantly in a surface-aligned state. This study indicates that the lytic activity of MK14-A430 occurred through a pore-forming mechanism. The lipid headgroup environment experienced by the fluorescent label, where MK14-A430 displayed pore information, indicated that pore formation was best described by the toroidal pore model.

1. Introduction

The development of antimicrobial (or antibiotic) resistance, which is the ability of microorganisms to prevent cell death by antimicrobial agents (i.e. antibiotics, antivirals), is an increasing problem facing the treatment of infectious diseases. Most antibiotic drugs target cell functions of the microorganisms responsible for infectious diseases, such as cell wall biosynthesis [1], protein synthesis [2–4] and cell replication (through attacking DNA) [5]. These functions involve features of bacterial cell structure that can be mutated through relatively minor processes to develop resistance to these drugs [6]. Therefore, new means of killing or disabling bacterial cells are required that circumvent the cells' ability to develop AMR.

1.1. Antimicrobial peptides

One of the avenues pursued in the fight against AMR is the application of naturally-occurring antimicrobial peptides [7, 8] that are sourced from plant and animal venoms or host-defence systems that are part of a species' immune response. These peptides display broad-spectrum cell-killing activity; the major pathway of antimicrobial activity for these peptides is to directly attack the lipid matrix of cell membranes thereby bypassing the means through which cells develop resistance. Some of the commonly-studied antimicrobial peptides are short-chain, α-helical peptides that include melittin [9], magainins [10], protegrins [11], cecropins [12] and alamethicin [13]. These peptides typically comprise hydrophilic (including cationic) and hydrophobic residues that are sequestered on either side of the helix, as viewed down the helix axis. Cell lysis can occur through a number of processes, such as the detergent-like micellisation of the membrane's lipid matrix or through transmembrane pore formation. Pores formed by these peptides disrupt the transmembrane electrochemical gradient, leading to an increase in water flow that is associated with cell swelling and osmolysis (cell death caused by a colloid osmotic mechanism) [14].

1.1.1. *Melittin*

One of the most widely studied α-helical antimicrobial peptides since its discovery [15],

melittin is the major active peptide constituent of venom from *Apis mellifera* (European honey bee). Melittin is a 26-residue peptide with the sequence GIGAVLKVLTTGLPALISWIKRKRQQ [16], a molecular weight of 2846 Da and a net charge of +6 at physiological pH. Melittin has been found to adopt different locations, orientations and association states within membranes depending on experimental conditions and membrane composition [17, 18]. Melittin has been shown to have potential applications as an antibacterial against a penicillin-resistant strain of *Staphylococcus aurens* [19] as well as having powerful inhibitory effects on the lyme disease spirochete [20] and HIV-1 [21].

In this study, the interactions of a proline-substituted, fluorescently-labelled analogue of melittin, named melittin P14K-A430 (MK14-A430), with lipid membranes consisting of 1,2-dipalmitoyl-sn-glycero-3-phosphatidylcholine (DPPC) were investigated.

1.2. Evanescent wave-induced fluorescence spectroscopy

In order to study the interactions of peptides with lipid membranes, one approach is to assemble a supported lipid bilayer on a solid substrate, and probe these interactions using methods that provide a level of surface-specificity, and that are capable of detecting and probing conformational changes and dynamics. Evanescent wave-induced fluorescence (EWIF) spectroscopic methods can provide this information [22]. Briefly, total internal reflection at the interface formed between two media of different refractive indices results in an evanescent (standing) wave being produced in the optically rarer medium, which decays exponentially with distance from the interface over 10s to hundreds of nanometres. A fluorophore within the evanescent wave region, acting either as a probe that locates in the interfacial region or is chemically attached to a surface-specific species of interest, can absorb energy from this field and hence be electronically excited, after which it can fluoresce, and thereby report on the properties of the system within the interfacial region to which it is sensitive. The EW selectively samples chromophores within its penetration depth, which can be varied by altering the angle of incidence of the excitation light, and thereby provides a means to probe properties that vary from the interfacial region to the bulk solution.

Time-resolved evanescent wave-induced fluorescence spectroscopy (TREWIFS) measurements provide additional information in the form of fluorescence decay kinetics of fluorescent species near an interface [23, 24]. The fluorescence decay kinetics can report on factors such as the polarity of the microenvironment of the fluorophore, and how such properties vary with distance from the interface.

Evanescent wave-induced fluorescence measurements can also be used for time-resolved fluorescence anisotropy measurements [22], i.e. EW-TRAMs. Such measurements are capable of probing emission depolarising events occurring in either, or both, planes parallel and perpendicular to that of the surface, thereby providing information such as the mobility of the fluorescent probe or fluorescently-labelled species in both planes. The use of EW methods is therefore an ideal approach to investigate the fluorescence reporters of the lytic activity of a peptide interacting with a supported lipid bilayer. As the membrane-water interface of SLBs is parallel to the surface at which they are formed, this provides EW-TRAMs with the ability to resolve depolarisation processes (including peptide motions) in different planes of the bilayer. Consequently, the location and mobility of the MK14-A430 peptide when in different states (i.e. surface-aligned or transmembrane pore-forming) may be observed by monitoring the fluorescence of the AlexaFluor 430 label monitored by time resolved, evanescent wave-induced fluorescence spectroscopy and anisotropy measurements using the unique interrogating capabilities of these EW approaches.

2. Experimental methods

2.1. Materials

2.1.1. Solution preparation

NaCl (99.5% pure) and hydrochloric acid (50%) were purchased from Merck Chemicals (Darmstadt, Germany). 4-(2-hydroxyethyl)-1-piperazineethanesulfonic acid (HEPES, 99% pure) was purchased from Acros Organics (Geel, Belgium). Milli-Q^{TM} water from a Millipore Type I reagent system (Millipore Corp, Bedford, USA) with a resistivity of 18.2 MΩ was used for all aqueous solution preparations and cleaning. Ethanol, Methanol, Propan-2-ol, Acetonitrile, Pyridine (all spectroscopy grade), were purchased from Merck Chemicals (Darmstadt, Germany). 1,2-Dipalmitoyl-sn-Glycero-3-Phosphatidylcholine (DPPC) and cholesterol (98%, ovine wool) were purchased from Avanti Polar Lipids (Alabaster, USA). DPPC is a 16:0 phospholipid with a phase transition temperature of 41 °C. The fluorescent label AlexaFluor 430 (A430) was purchased from Molecular Probes (Carlsbad, USA). All materials were used without further purification. HEPES buffer solution was prepared by dissolving 10 mM HEPES and 150 mM NaCl in Milli-Q^{TM} water. The solutions were adjusted to pH 7.4 using small amounts of concentrated (∼5 M) NaOH. All solutions of A430, native melittin or melittin P14K-A430 were prepared at concentrations of 5 μM. Concentrations were determined by measuring the absorbance of A430 (extinction coefficient at 430 nm = 15 000 M^{-1} cm^{-1} [25].

2.1.2. Cleaning materials and methods

Nitrogen (High Purity grade, 99.99%) was purchased from BOC Gases (Preston, Victoria, Australia). Extran® MA03 cleaning solution and nitric acid (70%) were purchased from Merck Chemicals (Darmstadt,

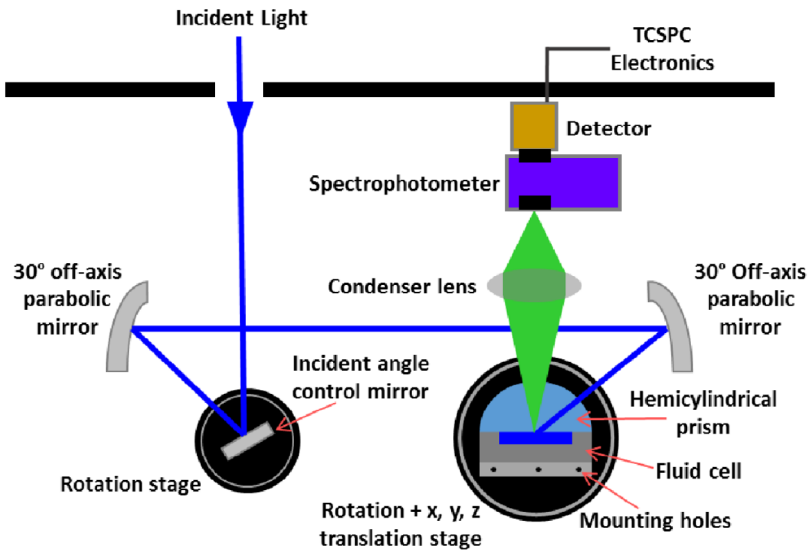

Figure 1. Schematic representation of the TREWIFS setup. Note the arrangement of the detection components is orthogonal to the interfacial plane.

Germany). All equipment was cleaned immediately prior to use. Stainless steel equipment, general glassware and plastics were cleaned by sonicating for 1 h in 10% Extran surfactant solution (to remove dirt, oils and other contaminants) followed by rinsing with copious amounts of Milli-Q^{TM} water. To remove residual surfactant and more strongly adsorbed contaminants required different procedures depending on the equipment. Stainless steel equipment was soaked in 10% nitric acid for a minimum of 12 h, while general glassware and plastics were soaked in warm, concentrated (~60 °C, ~5 M) NaOH for 4 h. After this round of cleaning, all equipment was again rinsed with copious amounts of Milli-Q^{TM} water. Plastics were boiled in Milli-Q^{TM} water one additional time for 10 min (to remove residual base and plasticisers) then rinsed with copious amounts of Milli-Q^{TM} water.

The hemicylindrical prisms used for TREWIFS experiments were cleaned by rinsing with copious amounts of Milli-Q^{TM} water, followed by soaking for up to 2 h in a warm ammoniacal peroxide solution (1:1 hydrogen peroxide and Milli-Q^{TM} water, with a few millilitres of concentrated ammonia) to oxidise residual organic contaminants non-corrosively [26]. The substrates were then rinsed with copious amounts of Milli-Q^{TM} water.

2.1.3. Peptide synthesis and fluorescent labelling

A430 was used for fluorescently-labelling the melittin derivative for several reasons: the emission characteristics of A430 shows sensitivity to the local environment polarity, its fluorescence and photostability are considerably greater than the alternative of exciting the native tryptophan chromophore and it shows no significant change in fluorescence when coupled to peptides. An additional benefit of A430 in studies using EWIFS is that A430 emission is reasonably insensitive insensitive to the presence of a silica interface (see other common fluorophores such as the Rhodamine family) [27].

Substituting the Pro-14 residue from native melittin for Lys provides the sequence GIGAVLKVLTTGL **K**ALISWIKRKRQQ-CONH$_2$. This substitution allows amine coupling of the A430 at the K14 position. The location of the fluorescent species near the N- and C-termini limits its ability to report on processes occurring at the middle of the helix. In the present study we have avoided this limitation by substituting the proline-14 residue with lysine to which the fluorescent label A430 is attached. The labelled Lys-14 residue lies near the middle of the peptide chain, close to the plane that separates the hydrophilic and hydrophobic regions of the amphiphilic helix. At this location the A430 label should protrude from the peptide helix where it can sample the peptide's microenvironment and thereby probe the location and mobility of MK14-A430 in SLBs of DPPC. Melittin and melittin P14K-A430 were prepared by solid-phase peptide synthesis [28] in the laboratory of Professor John Wade (Howard Florey Institute, University of Melbourne) as described elsewhere [29].

2.2. TREWIFS apparatus

The TREWIFS apparatus (figure 1) was constructed utilising a hemicylindrical fused silica prism design, which reduces the effects of refraction and spurious reflections within the prism compared to other prism shapes. The apparatus is based upon the design described previously [23, 30] with the modification of an open-faced stainless steel flow cell with an internal volume of 900 μl (height 12.5 mm, width 24 mm, depth 3 mm) clamped to the prism's optical face to allow for solution exchange (figure 2). The cell-prism junction was sealed by a Teflon sheet with a hole cut to the dimensions of the open face (height 12.5 mm by width

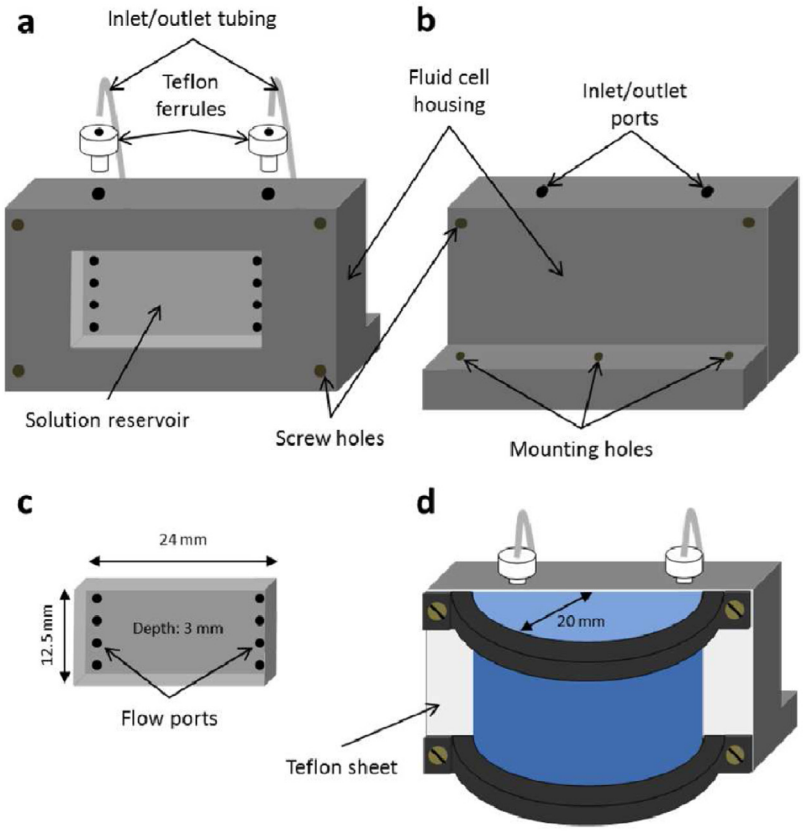

Figure 2. Schematic of the cell used for TREWIFS and EW-TRAMs experiments. The stainless steel flow-through fluid cell is shown from the front (a) and rear, (b). The mounting holes at the rear (b) allow the cell to be secured in place on the stage in the TREWIFS apparatus. The dimensions of the solution reservoir are shown in (c) and the complete, constructed cell in (d). The hemicylindrical prism is secured in place with two screw-in brackets and the fluid cell-prism junction is sealed by a Teflon sheet with a hole cut to the area of the solution reservoir.

24 mm). The solution within the flow cell was exposed to the prism's active surface via the open face.

The excitation source was a frequency doubled and cavity dumped, mode-locked Titanium:sapphire laser (Coherent Mira 900F-Verdi V-10, Pulse Switch) operating at 860 nm, with pulses of ~100 fs duration and a pulse repetition rate of 7.6 MHz. The emission following 430 nm excitation was detected orthogonal to the excitation path by a microchannel plate photomultiplier (MCP, Eldy model EM1-132) after passing through an emission polariser (King) set at the magic angle (54.7°), a fused silica f/1 condensing lens (Newport), a polarisation scrambler, a 495 nm cutoff filter to reject scattered excitation light and a single grating monochromator (Jobin Yvon, model H-20). The emission signal was monitored and recorded by conventional time correlated single photon counting (TCSPC) electronics [31]. The excitation signal (taken from either a high-speed photodiode detector or the synchronous output from the laser pulse selection electronics) and emission signal (taken from the MCP) were passed through constant fraction discriminators (Tennelec Quad TC 455). The time difference between excitation and emission events was measured by a time-to-pulse height converter (Ortec model 457) in 'inverted TAC mode' and multi-channel analyser (MCA, Viking Instruments (Norland) Model 5000).

The angle of incidence of the excitation beam normal to the silica-water interface (critical angle: 66.3°) was kept constant at 70° for all evanescent wave-induced fluorescence spectroscopic measurements, which corresponds to a penetration depth of 108 nm (assuming that the refractive index of the sample is similar to that of water).

2.2.1. Evanescent wave-induced time-resolved anisotropy measurements

The evanescent wave-induced time-resolved anisotropy measurements (EW-TRAMs) were performed using the TREWIFS apparatus described above. The polarisation-dependent fluorescence decay curves were acquired using TCSPC as described above, with the addition of a silica double-rhomb polarisation rotator (Halbo-Fresnel Rhomb) for selecting the polarisation of the excitation light, while the emission polarisation analyser mounted in the housing for the condenser lens selected fluorescence emission of a specific orientation. The polarisation analyser is mounted as the first optical component in the detection setup to minimise the effects of polarisation on other optical components (i.e. the emission collection lens). The emission polariser was controlled by a computer program that enabled collection of both emission polarisations in separate memory channels of the MCA, changing between

Table 1. Fluorescence lifetime distribution analysis results for MK14-A430 in different hydroxylic solvents.

Solvent	f_1	τ_1 (ns)	SD_1 (ns)	f_2	τ_2 (ns)	SD_2 (ns)	f_3	τ_3 (ns)	SD_3 (ns)
Water	0.02	0.3	0.01	0.12	1.6	0.07	0.86	4.0	0.58
HEPES	0.03	0.3	0.02	0.17	1.3	0.15	0.86	3.4	0.51
MeOH	—	—	—	0.03	2.1	0.05	0.97	4.9	0.12
EtOH	—	—	—	0.03	2.1	0.04	0.97	5.0	0.12

Note: SD_i corresponds to the standard deviation of the ith distribution peak. χ^2_R values for the analyses are 1.11, 1.21, 1.17 and 1.16 for water, HEPES, MeOH and EtOH respectively.

emission polarisations every 30 s. After the collection of the two fluorescence decays for one excitation polarisation orientation, the excitation polariser was manually rotated to obtain the other excitation-emission permutations. Fluorescence decay profiles were collected for each of these excitation-emission permutations over a set time period of 2 h (30 min total counting in each excitation-emission permutation) rather than to a preset maximum number of counts. Laser power and photostability of A430 were carefully monitored during an EW-TRAMs experiment and no detectable changes in either parameter were observed over the course of a single experiment.

3. Results and discussion

The fluorescence decay behaviour of A430 provides a polarity-sensitivity that will aid detection of the local environment of the probe and the peptide to which it is attached [29]. In contrast to free A430 in solution, the fluorescence decay behaviour of MK14-A430 was found to be biexponential: one lifetime component, τ_1, is shorter than the lifetime of A430 in solution, in the range 0.8–1.7 ns, and a longer lifetime component, τ_2, in the range 3.6–5.0 ns [29]. The range of lifetimes and polarity dependence of τ_2 is similar to that observed for free A430. The value of τ_2 is therefore a good sensor of the local environment of the peptide at the K14 position along the peptide chain. The value of τ_2 is greater than for free A430 in aqueous solvents, which may be due to the restriction of dielectric relaxation of water molecules in the proximity of the peptide, resulting in a decrease in the local dielectric constant [32].

The short decay component (τ_1) appears attributable to some interaction between the fluorophore and peptide, resulting in dynamic quenching of A430 fluorescence. The possibility of heterogeneous resonance energy transfer as the quenching process can be discounted since there are no chromophores that absorb in the region of A430 emission. Likewise, poor spectral overlap resulting from the large Stokes shift of A430 means that homogeneous fluorescence resonance energy transfer is unlikely. Dynamic quenching by chloride ions can be discounted as the short lifetime is also present in solutions with no electrolyte. It is possible that photoinduced electron transfer (PET) occurs [33, 34], however. PET between aliphatic amines and coumarins has been observed [35], suggesting that amines from the N-terminus as well as lysine and arginine side-chains may be responsible. However, these amines are protonated at the pH of the aqueous solutions, greatly reducing their ability to act as an electron donor in PET [36]. PET between photoexcited organic fluorophores and tryptophan has also been reported [37], though. It is possible that the peptide adopts a conformation that enables PET between the A430 probe and intrinsic tryptophan along the peptide chain.

In our previous work [29], the analysis of A430 fluorescence only considered the probe as existing in discrete states or environments, however, an amphiphilic peptide such as MK14-A430 presents an environment of chemical heterogeneity that may be sensed by the A430 probe, as will the lipid environments investigated in this study. In these cases, fluorescence lifetime distribution analysis can be used to investigate the diversity of the probe microenvironments. It should be noted that as the majority of lifetime distributions reported here were symmetrical, the lifetime peak is reported as the value of τ for simplicity. For the lower-polarity hydroxylic solvents, the lifetime distribution analysis returned two narrow (low standard deviations, SD) components with similar results to the discrete biexponential fit (table 1), indicating that the discrete two-exponential model was an appropriate representation of that data. In contrast, three components were determined for the aqueous solution decays, with broader lifetime distributions.

The shorter lifetime peak (0.3 ns) indicated that another state or conformation exists, which is more efficiently quenched than those in the lower-polarity hydroxylic solvents. The possibility of heavy-ion collisional quenching can again be discounted due to the short component's presence in Milli-Q^{TM} water, where no electrolyte is present. It is possible that the two quenched decay components might represent intra- and intermolecular PET quenching pathways, though further investigation is required to deduce its origin.

It appears that the changes in fluorescence decay kinetics could arise from different conformations of MK14-A430. Another possibility is that the distinct lifetimes represent different locations of the fluorophore with respect to the peptide conformation. A third possibility is that quaternary interactions can change the proportion of different components (lifetimes) through peptide-peptide interactions. However, we did not find a simple relationship between the polarity and the fractional contributions. The main conclusion we draw from our time-resolved studies is that the fluoro-

Table 2. Results from the discrete lifetime analysis of MK14-A430 free in HEPES solution and interacting with DPPC and DPPC-Chol SUVs (L:P in brackets).

System	f_1	τ_1 (ns)	f_2	τ_2 (ns)	χ^2_R
Free MK14-A430	0.16	0.8	0.84	3.6	1.26
DPPC (10:1)	0.06	1.6	0.94	4.6	1.12
DPPC (20:1)	0.13	2.4	0.87	4.8	1.21
DPPC (100:1)	0.06	2.3	0.94	5.0	1.16
DPPC-Chol (10:1)	0.19	1.0	0.81	3.5	1.37
DPPC-Chol (20:1)	0.19	1.0	0.81	3.5	1.26
DPPC-Chol (100:1)	0.21	0.9	0.78	3.5	1.65

phore lifetime is a probe of solvent polarity and changes in peptide conformation that may accompany peptide-lipid or peptide-surface interactions.

3.1. Melittin P14K-A430 interactions with lipid bilayers

3.1.1. DPPC SUVs

The time-resolved fluorescence decays of MK14-A430 interacting with DPPC SUVs showed multiexponential behaviour (data not shown), like the free peptide. However, the fluorescence decay kinetics were slowed in the presence of DPPC SUVs. The simplest analysis that provided good fits to the data consisted of a sum of two exponential components (table 2). This returned fluorescence lifetimes of $\tau_1 = 1.6$–2.4 ns and $\tau_2 = 4.6$–5.0 ns. The lifetime distribution analysis provided two distributions for all L:P (table 3), with similar values to the discrete fit: $\tau_1 = 1.7$–2.1 ns and $\tau_2 = 4.5$–5.0 ns. Attempting a global discrete lifetime analysis with common fluorescence lifetimes returned poor fits ($\chi^2_R > 1.5$, non-random residuals at short timescales), likely due to the polarity sensitivity of both the quenched and unquenched species.

The value of τ_1 is smaller than the values for all unquenched, solvent-exposed A430 species, including the most polar environment (free probe in water, $\tau = 3.2$ ns). This indicates that τ_1 again corresponds to a PET-quenched population of A430. The values of τ_1 and τ_2 are similar to those corresponding to the lower-polarity solvents. This suggests that the probe has penetrated into the structure of the lipid bilayer, likely to be a deeper part of the interfacial region (i.e. carbonyl) due to its similar polarity range ($\epsilon = 10$–30) to the lower-polarity solvents studied here ($\epsilon \approx 12$–37). None of the values of τ_1 and τ_2 indicated an aqueous probe environment, though an increase in polarity was observed with decreasing L:P (increasing peptide). This polarity increase was accompanied by a broadening of both fluorescence lifetime peaks.

Peptide accumulation on the surface could also explain the trends observed. According to the Shai-Matsuzaki-Huang model [38–40], peptide association involves lipid headgroup displacement and peptide incorporation into the bilayer interfacial region. This is likely to cause increased water penetration and freedom for probe fluctuations, which could explain both the shorter lifetimes and broader lifetime distributions with decreasing L:P (increasing peptide accumulation within the SUVs).

Table 3. Fluorescence lifetime distribution analysis results for MK14-A430 in DPPC and DPPC-Chol SUVs.

System	DPPC			DPPC-Chol		
(L:P)	10:1	20:1	100:1	10:1	20:1	100:1
f_1	0.05	0.06	0.05	0.03	0.05	0.07
τ_1 (ns)	1.7	1.8	2.1	0.4	0.5	0.6
SD_1	0.08	0.11	0.05	0.10	0.04	0.01
f_2	0.95	0.94	0.95	14	24	25
τ_2 (ns)	4.5	4.6	5.0	1.1	1.6	0.21
SD_2	0.47	0.60	0.24	0.30	0.21	0.05
f_3	—	—	—	0.83	0.71	0.68
τ_3 (ns)	—	—	—	0.83	0.71	0.68
SD_3	—	—	—	0.74	0.45	0.11
χ^2_R	1.28	1.26	1.16	1.18	1.19	1.32

3.1.2. DPPC-Chol SUVs

When MK14-A430 was associated with DPPC-Chol SUVs, the fluorescence decay profiles were similar to those for free MK14-A430 at all L:P (data not shown). Biexponential discrete analysis returned lifetime values that are similar to that for the free peptide (table 2). However, this analysis resulted in fits with non-random residuals at short timescales and poor fits ($\chi^2_R > 1.5$), suggesting more complex decay kinetics. Therefore, only the lifetime distribution analysis results (table 3) will be discussed here. The lifetime distribution analysis returned three lifetime peaks: $\tau_1 = 0.4$–0.6 ns, $\tau_2 = 1.1$–1.6 ns and $\tau_3 = 3.5$–3.8 ns. The value of τ_1 decreases with L:P and at 10:1, is close to that for free MK14-A430 in aqueous solution. This indicates that quenching is polarity-dependent, supporting the idea that this contribution is due to another PET mechanism. The contributions from the quenched lifetimes were greater at all L:P when compared with the pure DPPC SUV systems. Like the pure DPPC systems, lowering the L:P results in lifetime distribution peak broadening for all components.

Therefore, the key differences for the DPPC-Chol SUV systems when compared with DPPC SUVs were a probe microenvironment of higher polarity and greater probe quenching. There is no apparent correlation between peptide secondary structure and these parameters according to circular dichroism experiments performed on these systems (data not shown). Attempts to use a fixed, 4 exponential component fit could not determine separate contributions from free/bound peptide, due to the similar decay kinetics to free MK14-A430. Thus, it appears that the differences were due to the location of the probe (and peptide) within the SUVs.

It may be that the penetration of A430 into the SUV structure may explain the differences. The indole ring of tryptophan is known to take a position near the carbonyl moiety of the interfacial region and behave as an 'interfacial anchor' for membrane-incorporated pep-

Table 4. Results to the two-exponential discrete fluorescence lifetime analysis for fluorescence decay kinetics recorded under TREWIFS conditions at a silica-HEPES solution interface.

System	f_1	τ_1 (ns)	f_2	τ_2 (ns)	χ^2_R
A430	—	—	1.00	3.1	1.03
Free MK14-A430	0.57	0.9	0.43	3.3	1.17
DPPC SLB (overnight)	0.40	1.2	0.60	3.7	1.16
DPPC SLB (equilibrium)	0.20	0.9	0.80	3.5	1.31
DPPC-Chol SLB	0.58	1.0	0.42	3.2	1.67

tides [41–43]. This region was described earlier as having moderate polarity (similar to that suggested for pure DPPC SUVs) and high motional restriction. In contrast, studies of the intrinsic tryptophan residue of native melittin [44] and NBD-labelled melittin [45] into DOPC bilayers showed a shallower position within the lipid bilayer structure, resulting in greater motional freedom and environment polarity when cholesterol was present.

Shallower penetration of A430 into the SUV structure could explain the higher environment polarity, potentially due to increased water penetration. The greater motional freedom may explain the greater extent of quenching as it has been observed that in structures with restricted conformational mobility PET is reduced [46]. This is understandable due to the exponential distance-dependence of PET [47–49].

3.1.3. Time-resolved evanescent wave-induced fluorescence spectroscopy (TREWIFS)

The fluorescence decay of A430 under TREWIFS conditions has been shown to be monoexponential with a decay time of 3.1 ns, indicating no discernible change in the fluorescence decay kinetics of A430 between bulk solution and at the silica-water interface [29]. This is expected, as the silica-HEPES buffer interface is highly polar. In comparison, many other common fluorescent probes exhibit significant changes in their emission properties when in close proximity to a silica interface. The insensitivity to the silica surface indicates the value of A430 as a probe of interfacial environments.

In contrast to the free (non-complexed) A430, the fluorescence decay behaviour of melittin P14K-bound A430 (table 3) changed at the silica-HEPES solution interface (table 4). The data were suitably fit using a biexponential decay analysis, with similar values of τ_1 and τ_2 as free MK14-A430 in HEPES solution. However, the value of f_1 was larger relative to its contribution in bulk solution: 0.16 in bulk solution, 0.57 at the silica-HEPES interface. This indicates that the peptide adopted a conformation that exhibited significantly greater PET quenching than in free solution.

3.1.4. TREWIFS of Melittin P14K-A430 with DPPC SLBs

Previous TREWIFS and EW-TRAMs investigations of MK14-A430 interacting with a pure DPPC SLB have been published [29] in which MK14-A430 was incubated with the DPPC SLB overnight (~12 h). However,

Table 5. Results of the fluorescence lifetime distribution analysis for fluorescence decay kinetics of MK14-A430 interacting with SLBs recorded under TREWIFS conditions.

System	DPPC SLB (overnight)	DPPC SLB (equilibrium)	DPPC-Chol SLB (equilibrium)
f_1	0.07	0.05	0.47
τ_1 (ns)	0.2	0.5	0.7
SD_1	0.01	0.01	0.07
f_2	0.33	0.14	0.30
τ_2 (ns)	1.2	1.2	1.8
SD_2	0.08	0.05	0.13
f_3	0.60	0.56	0.23
τ_3 (ns)	3.7	3.0	3.7
SD_3	0.18	0.15	0.16
f_4	—	0.25	—
τ_4 (ns)	—	4.9	—
SD_4	—	0.19	—
χ^2_R	1.38	1.10	1.41

QCM-D experiments, performed subsequent to the publication of the initial findings, indicated that the incubation time required to reach an equilibrium state was 72 h (to be published). Experiments were therefore reperformed using this 72 h peptide incubation period. The fluorescence decays recorded after the overnight incubation of MK14-A430 with a DPPC SLB (table 4) displayed faster kinetics than free MK14-A430 in HEPES solution. The data were still well-fit by a biexponential decay model. This was reflected in the discrete lifetime analysis, which returned a substantial (0.40) fractional contribution for the quenched component, τ_1. However, the values of τ_1 and τ_2 increased relative to the peptide in bulk solution or at the silica-HEPES interface, indicating that the probe experienced an environment of lower polarity when associated with the SLB. The logical explanation for this is some partitioning of A430 into the SLB structure.

The decays recorded after the SLB-peptide system had reached equilibrium (table 4) showed a decrease in the contribution of τ_1 to $f_1 = 0.20$, with shorter lifetimes for both τ_1 and τ_2. This indicated changes in peptide arrangement (from the overnight-incubated stage) that resulted in a higher polarity sensed by A430 but a lower extent of quenching occurring. The value of τ_{ave} increased from 2.7 ns after overnight incubation to 3.0 ns following equilibration. This was in contrast to the decrease in τ_{ave} with incubation time observed for MK14-A430 interacting with DPPC giant unilamellar vesicles (GUVs) [50]. In the study involving GUVs, the decrease in τ_{ave} was attributed to an increase in PET-quenching events that were assigned to a lytic pore state. It is likely that more MK14-A430 associated with the SLB between 12 and 72 h. Therefore, in light of studies performed here and other studies that show an increase in I-state peptide with membrane-bound peptide concentration [51], it would seem counterintuitive that the extent of pore formation decreased.

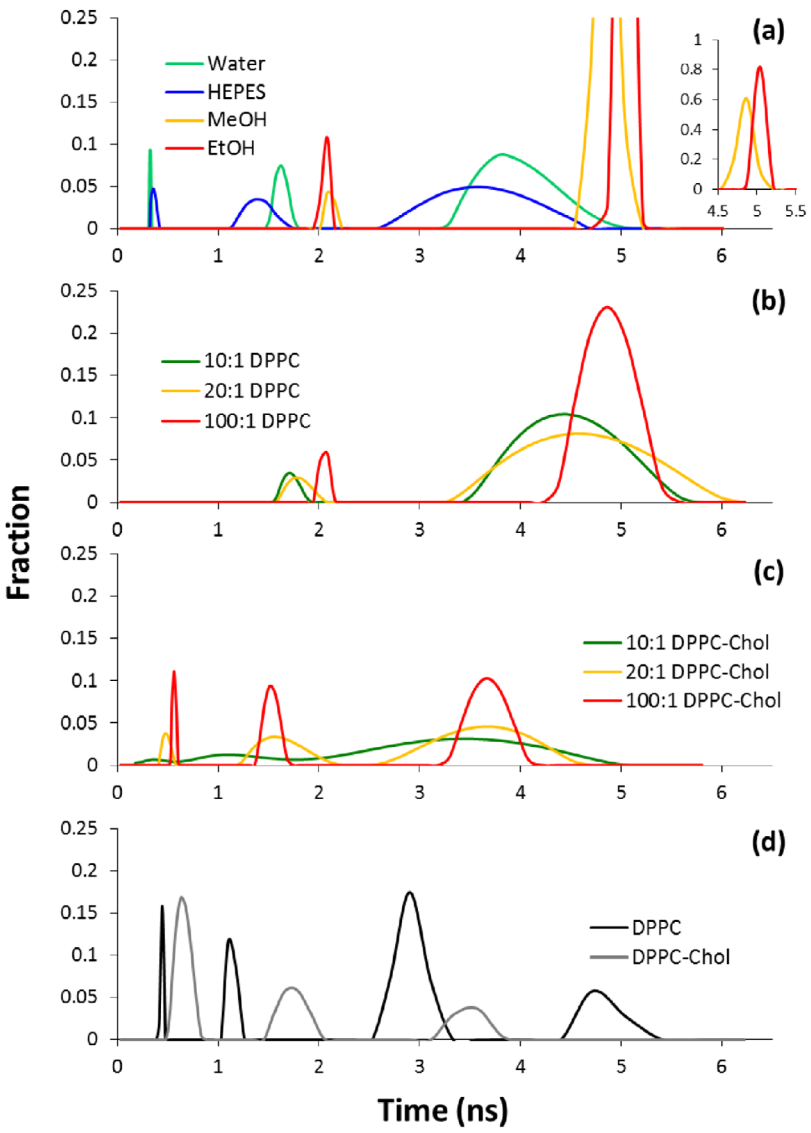

Figure 3. Results from fluorescence lifetime distribution analysis of melittin P14K- A430 (a) in different hydroxylic solvents and interacting with (b) pure DPPC vesicles, (c) DPPC-Chol SUVs and (d) DPPC and DPPC-Chol SLBs (at equilibrium). Inset in (a): plot of τ_2 contribution for free MK14-A430 in methanol and ethanol.

The results from the lifetime distribution analysis (table 5, figure 3) may provide some insight into these changes. The DPPC SLB:MK14-A430 system at equilibrium returned four components from the distribution analysis: 0.5 ns, 1.2 ns, 3.0 ns and 4.9 ns. It should be noted that while there is an improvement in the fit between the discrete biexponential fit and the lifetime distribution fit, the data are still reasonably fit by the discrete biexponential model. It should also be noted that the distribution analysis did not provide a better fit to the overnight-incubated data (tables 4 and 5 for overnight-incubated data) and is not discussed alongside the distribution fit to the equilibrium system. The data for the overnight-incubated system in table 5 are included for comparison only.

The distribution analysis indicated that the probe partitioned into polar (3.0 ns unquenched, 0.5 ns and 1.2 ns quenched) and non-polar (4.9 ns) environments. The 4.9 ns component is similar to that observed for MK14-A430 associated with DPPC SUVs at L:P = 100:1, where no evidence of pore formation was observed [52]. This suggests that this population of the probe corresponded to peptide in the S-state. The polar environment experienced by the rest of the probe population indicates that it is not embedded within the bilayer structure, suggesting a pore-forming state. Therefore, it appears that a combination of S- and I-state peptide is reported by the TREWIFS fluorescence decay.

3.1.5. The influence of cholesterol

All comparisons made here involve only the pure DPPC and DPPC-Chol SLB systems at peptide association equilibrium (unless stated). The TREWIF signal from MK14-A430 interacting with a DPPC-Chol SLB decays faster overall compared with the pure (absence of cholesterol) DPPC SLB. The discrete exponential analysis (table 4) returns values of $\tau_1 = 1.0$ ns and $\tau_1 = 3.2$ ns, with both lifetimes indicating that the probe experiences an environment of polarity similar to

aqueous solution. The contribution of τ_1 (0.58) indicates that more fluorescence quenching events occurred than in the pure DPPC SLB. However, the fit returns a χ^2_R of 1.67 with non-random residuals, indicating that a two discrete environment representation does not model the data well.

The distribution analysis (table 5, figure 3) of the DPPC-Chol SLB system returned three lifetime peaks: values of 0.7 ns, 1.8 ns and 3.7 ns. These fluorescence lifetimes were all consistent with an environment of moderate polarity. A greater extent of quenching occurred than in the DPPC SLB, similar to the change observed between the DPPC and DPPC-Chol SUV systems. These results suggest a shallow interfacial region location (i.e. lipid headgroups) for the probe, as was suggested for the DPPC-Chol SUV systems.

All of the fluorescence lifetimes indicate an environment of similar polarity. It is tempting to suggest a single state of peptide arrangement, (i.e. S-state), which would be supported by the ability of cholesterol-containing membranes to resist peptide transmembrane insertion [53]. However, more information is required to confirm this.

3.1.6. *Time-resolved fluorescence anisotropy measurements (TRAMs)*

TRAMs decays were also measured for MK14-A430 in HEPES solution and in the presence of pure DPPC and DPPC-Chol SUVs. The time-resolution of such data provides the ability to monitor probe and peptide motional dynamics. A free fluorophore will typically undergo fast motions resulting in rapid depolarisation of emission leading to low values of the fluorescence anisotropy. In the simplest of cases such as a spherical fluorophore rotating uninhibited, the time-dependent anisotropy decay, $r(t)$, may be represented as:

$$r(t) = r_0 e^{\frac{-t}{\phi_f}} \tag{1}$$

where ϕ_f is the rotational correlation time of the fluorophore. For sake of simplicity, A430 is assumed to have motion similar to a spherical fluorophore. This is due to its small size, meaning that rotations along different axes that may depolarise fluorescence at different rates cannot be satisfactorily resolved with the experimental setup used in this study.

When attached or associated to an object, the probe's fluorescence anisotropy time-dependence becomes more complex. This association or attachment may limit the angular range of fluorophore rotation, meaning that the anisotropy will not decay to zero. In this case, the anisotropy decay may be represented by the hindered rotator model [54–56]:

$$r(t) = (r_0 - r_\infty) e^{\frac{-t}{\phi_f}} + r_\infty \tag{2}$$

where r_∞ is the non-zero anisotropy value that can be observed at times beyond those of the fluorescence intensity decay. The hindered rotator model is a simplified expression that assumes that the anisotropy decay is exponential. If the object to which the fluorophore is attached (i.e. a small peptide such as melittin P14K) has molecular motions that can be resolved within the timeframe of the probe's fluorescence intensity decay, then the anisotropy will also reflect peptide motions. In this case, r_∞ can be replaced by a term representing the extent of depolarisation due to peptide motion, as follows:

$$r(t) = r_0 \left[\alpha e^{\frac{-t}{\phi_f}} + (1-\alpha) e^{\frac{-t}{\phi_p}} \right] \tag{3}$$

where ϕ_p is the correlation time relating to whole-body motions of the peptide to which the fluorophore is attached. In this case, the anisotropy at time t is dependent upon the degree of depolarisation due to fluorophore and peptide motions, with amplitudes of $r_0\alpha$ and $r_0(1-\alpha)$, respectively. Therefore, if the peptide itself is a freely-diffusing body with a rotational correlation time comparable to the fluorescence lifetime of the probe, the anisotropy will decay to zero. If the motions of the fluorophore are indeed hindered by its attachment to the peptide ($\alpha < 1$), a multi-exponential decay will be observed for $r(t)$. This is considered a strong possibility for these studies due to the location of the A430 probe near the centre of the melittin P14K helix. It has been established that a fluorophore location near the centre of a peptide helix—where peptide backbone fluctuations are less—results in more hindered fluorophore fluctuations [57]. If the fluorophore motions are not hindered by its attachment, an apparently single-exponential decay would be observed, with a correlation time; $\phi_a = \frac{\phi_f \phi_p}{(\phi_f + \phi_p)}$. Thus, the motion of the fluorophore would only be observed by the short timescale of ϕ_a relative to that expected for peptide rotation.

It is more elegant to represent the extent of depolarisation due to fluorophore and peptide motions as fractional contributions of short and long correlation times ($f_s = \alpha$ and $f_L = (1-\alpha)$), such that:

$$r(t) = r_0 \left(f_s e^{\frac{-t}{\phi_s}} + f_L e^{\frac{-t}{\phi_L}} \right) \tag{4}$$

where the relationships between ϕ_s, ϕ_L and ϕ_f, ϕ_p are given by [58]:

$$\frac{1}{\phi_s} = \frac{1}{\phi_f} + \frac{1}{\phi_p} \text{ and } \frac{1}{\phi_L} = \frac{1}{\phi_p} \tag{5}$$

In this case, ϕ_L is equal to the rate of depolarisation due to peptide motions. However, ϕ_s only relates to the fluorophore depolarisation rate when $\phi_f \ll \phi_p$. Otherwise, a combination of fluorophore and peptide motions, described in equation (5) will be observed for ϕ_s.

3.1.7. *TRAMS of MK14-A430 in HEPES solution*

The anisotropy decay for free MK14-A430 in HEPES was complex (figure 4), displaying multiexponential behaviour. This indicates a combination of hindered

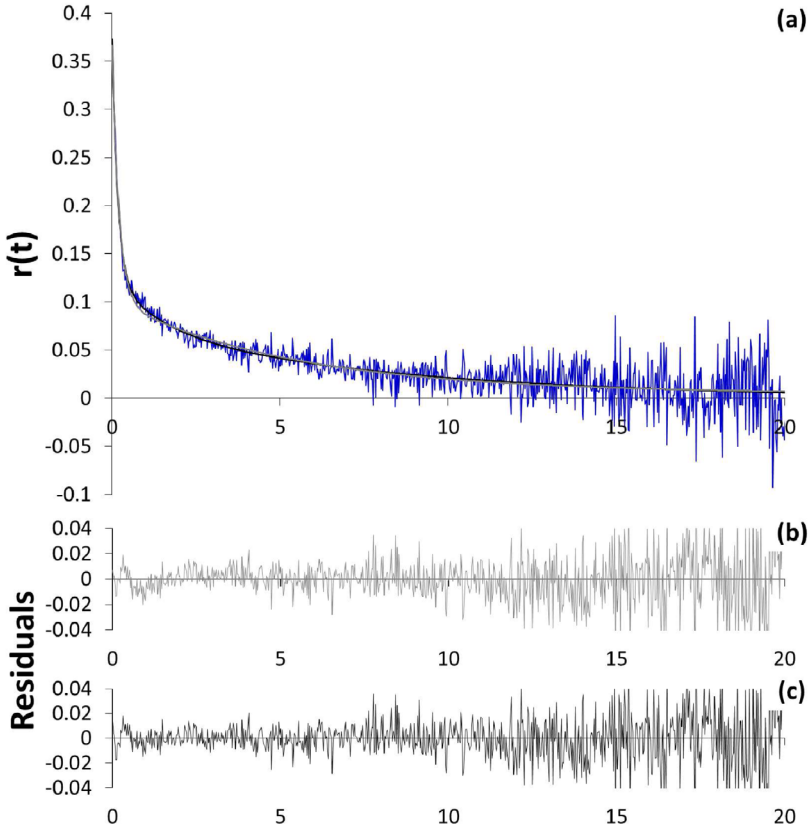

Figure 4. (a) Fluorescence anisotropy decay of MK14-A430 in HEPES solution. The 2-exponential (grey) and 3-exponential (black) fits to the data are displayed with the data, along with the residuals for the respective fits ((b) and (c)).

fluorophore motion around its point of attachment and peptide rotation. The results of the anisotropy decay analysis for MK14-A430 (free and associated with DPPC SUVs) are presented in table 6. The value of r_0 was 0.36, slightly lower than the calculated r_0 for A430 of 0.38. This suggests that some of the fast depolarisation processes were not completely resolved. The anisotropy decays to zero, as expected for a free, small peptide in an aqueous medium. Attempts to fit the data with two exponentials (equation (4)) could not accurately model the depolarisation behaviour, displaying non-random residuals (figure 4(b)). In fluorescence anisotropy decays recorded for native melittin [59], a third exponential component was observed to improve the fit quality for solutions under oligomeric but not monomeric conditions. Therefore, another 'long' component, represented by f_{L2} for fractional contribution and ϕ_{L2} for correlation time, was included into the fit.

The three-exponential analysis returned correlation times of $\phi_s = 0.2$ ns, $\phi_L = 1.4$ ns and $\phi_{L_2} = 7.9$ ns. Due to the large differences in magnitude between these correlation times, it is believed that there is little coupling between rotational modes as described by equation (5). Values in the range of 100–200 ps have been commonly observed for fluctuations of tryptophan around the point of attachment [57, 60, 61]. Therefore, ϕ_s is assigned to relatively free motions of the A430 at the end of the lysine sidechain. Motions of monomeric native melittin have been determined to have correlation times of 1.1–1.8 ns [60, 62, 63] similar to ϕ_L. A contribution of monomeric MK14-A430 is likely to be small as suggested from the high helicity of MK14-A430, meaning that ϕ_L may be reporting helix backbone fluctuations rather than whole-body diffusion. It is possible then, that the longer 7.9 ns correlation time is due to motions of an oligomeric form of MK14-A430. However, the largest known oligomer of native melittin is the tetramer, which has been associated with shorter rotational correlation times of 3.7–4.0 ns [60, 62, 63]. One possibility for this longer correlation

Table 6. Results of application of rotating fluorophore model to TRAMs measurements of MK14-A430 depolarisation free in HEPES solution and associated with pure DPPC SUVs at different L:P.

System	Free MK14-A430	DPPC (10:1)	DPPC (20:1)	DPPC (100:1)
r_0	0.36	0.4	0.39	0.32
f_s	0.66	0.34	0.31 (0.19)	0.38 (0.22)
ϕ_s	0.17	0.24	1.1 (2.3)	1.5 (2.2)
f_L	0.14	0.40	0.69 (0.81)	0.62 (0.78)
ϕ_L	1.4	1.5	8.3 (∼100)	11 (∼100)
f_{L2}	0.2	0.26	—	—
ϕ_{L2}	7.9	9.2	—	—
r_∞	0	0.12	0.25 (0)	0.19 (0)

Note: Results from the unrestricted rotator model fit are in brackets.

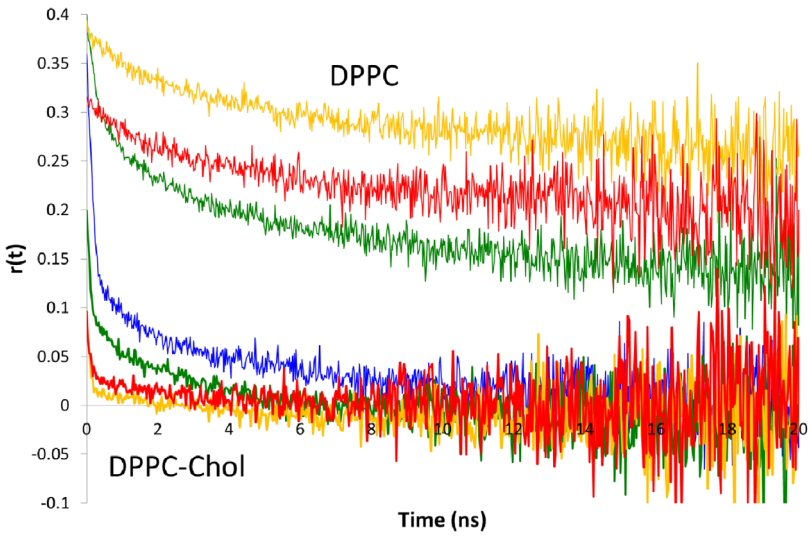

Figure 5. Time-resolved fluorescence anisotropy curves of melittin P14K-A430 free in solution (blue line) and interacting with DPPC SUVs (fine lines, top) and DPPC- 30 mole % cholesterol (thick lines, bottom) at lipid:peptide ratios of 10:1 (green), 20:1 (yellow) and 100:1 (red).

time is that the rod-like helix (due to the P14K substitution) accommodates MK14-A430 achieving higher order aggregates. Dynamic light scattering experiments performed on melittin P14A determined an average hydrodynamic radius of 1.8 ± 0.2 nm under fully-aggregated conditions (compared with 1.0 ± 0.1 nm for tetrameric melittin) [64]. In the same study, a cooperative oligomerisation model [65] applied to CD data determined that melittin P14A aggregates consisted of 9 ± 1 monomers. To compare with the light scattering result, the Stokes–Einstein–Debye equation [58] (equation (6)) was used to estimate the hydrodynamic radius of MK14-A430, assuming that the 7.9 ns term corresponded to the rotational correlation time for a spherical rotor:

$$\phi = \frac{\eta V_{\mathrm{m}}}{k_{\mathrm{B}} T} \tag{6}$$

where η is the viscosity of the medium, V_{m} is the molecular volume, k_{B} is Boltzmann's constant and T is temperature. Under the conditions described earlier, substituting the correlation time of $\phi_{L_2} = 7.9$ ns yields a hydrodynamic radius for MK14-A430 of 2.0 nm, which is within experimental error of light scattering experiments.

However, it is unlikely that an aggregate of such peptides exists in a spherical configuration. A cylinder might be a better representation of an oligomer comprised of rigid, rod-like helices of MK14-A430, as has been suggested for hexamers of model amphiphilic peptides [61]. To model the rotational diffusion of a cylindrical structure (as estimated using hydrodynamic theory [61, 66]) requires accounting for the ends of the cylinder [67–70], which becomes a greater factor as the aspect ratio, ρ (ratio of cylinder length, L to diameter, d; $\rho = \frac{L}{d}$) decreases. The rotational diffusion coefficients along and about the axis of symmetry of a cylinder are:

$$D_r^{\perp} = \left(\frac{3k_{\mathrm{B}}T}{\pi\eta_0 L^3}\right)(\ln\rho + \delta_{\perp}) \tag{7}$$

$$D_r^{\parallel} = \left(\frac{4k_{\mathrm{B}}T}{A_0\pi\eta_0 L d^2}\right)(\ln\rho + \delta_{\parallel}) \tag{8}$$

where $A_0 = 3.841$ and $\delta_{\perp}$ and $\delta_{\parallel}$ are the end-effect corrections, approximated using the method used by Hu *et al* [61]. The length of a magainin helix (3.45 nm) [71, 72] was used for L, due to the proline deficiency similar to melittin P14K. The value of ρ was estimated as the value at which the average correlation time (ϕ_{avg}) for diffusion along each of the three axes was equal to 7.9 ns. ϕ_{avg} was considered a reasonable estimate due to the closely-matched dimensions, as a value of $\rho = 1.03$ returned for this analysis. This value of ρ corresponded to a cylinder diameter of 3.4 nm. Using the typical estimate of a α-helical peptide helix diameter (1.0–1.1 nm) [73] for MK14-A430, and assuming a simplified space-filling model, a diameter of 3.4 nm was best approximated by an octomer of the peptide.

3.1.8. TRAMS of MK14-A430 associated with DPPC SUVs

The fluorescence anisotropy curves for the pure DPPC system (figure 5, table 6) show a significant degree of restriction to the motion of A430 compared to it being free in solution, on the timescale of the fluorescence intensity. In this case, the hindered rotator model (equation (2)) was applied to analyse the data. A single exponential function was insufficient to model the data and so a two-exponential hindered rotor model was applied:

$$r(t) = (r_0 - r_\infty)\left(f_s e^{\frac{-t}{\tau_f}} + f_L e^{\frac{-t}{\tau_p}}\right) + r_\infty \tag{9}$$

The shape of the anisotropy decays for 20:1 and 100:1 DPPC:MK14-A430 are similar, with no sub-

Table 7. Results of application of rotating fluorophore model to TRAMs measurements of MK14-A430 associated with DPPC-Chol SUVs at different L:P.

System	Free MK14-A430	DPPC (10:1)	DPPC (20:1)	DPPC (100:1)
r_0	0.36	0.2	0.09	0.09
f_s	0.66	0.51	0.71	0.71
ϕ_s	0.17	0.10	0.09	0.09
f_L	0.14	0.12	0.29	0.29
ϕ_L	1.4	0.72	2.6	2.5
f_{L2}	0.2	0.37	—	—
ϕ_{L2}	7.9	4.2	—	—
r_∞	0	0	0	0

Note: The results to the analysis of the free MK14-A430 fluorescence anisotropy decay are shown for reference.

nanosecond decay apparent as was observed with free MK14-A430. This is supported by the low emission quenching observed through the fluorescence lifetime decays and agrees with the higher steady-state anisotropy and REES values observed (data not shown). The observed values of r_0 are less than 0.40 for these decays. The value of r_0 decreases with increasing L:P: 0.40, 0.39 and 0.32 for 10:1, 20:1 and 100:1, respectively. As the peptide concentration was kept constant in these experiments, the vertical offset in r is believed to be due to increased scatter from the greater vesicle concentration.

A range of fit parameters can be used to provide a suitable fit for the L:P = 20:1 and 100:1 anisotropy decay profiles. The two extremes were considered to provide the range of parameters—the highest restriction to motion possible and unrestricted diffusion of the probe and peptide. For the high restriction case, r_∞ is fixed at the limiting anisotropy where the fluorescence intensity approaches zero, returning values of $\phi_s = 1.1$ (20:1), 1.5 (100:1) ns and $\phi_L = 8.3$ (20:1), 11 (100:1) ns, and $r_\infty = 0.25$ (20:1) and 0.19 (100:1). Fixing $r_\infty = 0$ results in longer correlation times: $\phi_s = 2.3$ (20:1), 2.2 (100:1) ns and $\phi_L \approx 100$ ns for both systems.

The absence of a sub-nanosecond correlation time suggests that A430 does not diffuse within an aqueous environment. The value of ϕ_s (~2 ns) is similar to that attributed to probe fluctuations near the water-membrane interface [74]. This result agrees with the assignment of a probe location embedded within the interfacial region.

The large range of values that can be assigned to ϕ_L makes a definitive interpretation difficult. However, the results of the fluorescence lifetime analysis suggest that the assignment can be made to motions in a lipid environment. The value of ϕ_s has already been assigned to probe fluctuations at the end of its attachment. Rigid-body rotational diffusion for transmembrane peptides has been estimated to be on the order of microseconds [75, 76] and is unlikely to be resolved on the timescale of this experiment. It is likely, then, that the values correspond to fluctuations of the entire peptide structure. Values close to those of the lower limit (8–11 ns) were attributed to backbone fluctuations of a polypeptide analogue of alamethicin traversing a lipid bilayer [57, 77]. Values between the lower and the upper limits (<100 ns) have been reported for peptide backbone fluctuations for different amphiphilic peptides within a lipid bilayer [59, 74, 78, 79]. Therefore, the value of ϕ_L appears to report on helix backbone fluctuations in a lipid environment.

When the L:P is further decreased (L:P = 10:1) the anisotropy decay kinetics change significantly. The anisotropy decay profile appears to have a shape that is somewhere between the higher L:P and free peptide decays. Similar to free MK14-A430, three exponential components are required to fit the data well. A fast depolarisation component ($\phi_2 = 240$ ps) was evident that is not apparent in the 20:1 and 100:1 systems. The values of the two longer correlation times (1.5 and 9.2 ns) are also shorter than either of the correlation times for the 20:1 and 100:1 systems. The value of r_∞ (0.12) indicates that highly-restricted or very slow peptide fluctuations were still observable. Interestingly, all three correlation times are similar to those for free MK14-A430, suggesting a coupling of free and SUV-associated peptide depolarisations (equation (5)).

3.1.9. TRAMS of MK14-A430 associated with DPPC-Chol SUVs

The fluorescence anisotropy decays considerably faster for all DPPC-Chol SUV systems (figure 5, table 7) than the pure DPPC SUVs or free MK14-A430. The anisotropy decay profiles for L:P = 100:1 and 20:1 appear dominated by sub-nanosecond processes with the fluorescence completely depolarised in <5 ns. The anisotropy decay for the 10:1 system was slower than the other L:P and was completely depolarised in <10 ns. The shape of the 10:1 decay appeared similar to that of free MK14-A430 and suggested a possible contribution from free peptide, as was suggested for the pure DPPC system.

As the fluorescence is observed to completely depolarise for all L:P, no r_∞ term is required to fit the data. The data for the 20:1 and 100:1 systems require two exponential components for an acceptable fit, while the 10:1 system requires three exponential terms (table 7). Analysis of the 20:1 and 100:1 DPPC-Chol decays returned values of $\phi_s = 90$ ps ($f_1 = 0.71$) and $\phi_L = 2.5$ ns ($f_2 = 0.29$). The timescales of these processes suggest probe fluctuations at the end of its attachment, free in solution (90 ps) and near a water-membrane interface (2.5 ns). The fractional contributions indicate that the depolarisation appears to be dominated by probe fluctuations at the end of its attachment that are not hindered by its environment (lipid or peptide). This would support the notion that A430 motional freedom within lipid bilayers was a significant factor in PET quenching efficiency. The value of r_0 (0.09) for both systems indicated a large degree of unresolved depolarisation, which could be explained by the predominant rapid depolarisation component. It appears reasonable to assume no

coupling of the 90 ps and ~2.5 ns components, as there is more than an order of magnitude difference in the timescales.

For the 10:1 system, it is likely that the $\phi_s = 100$ ps term is also due to probe fluctuations at the end of its attachment. However, the values of ϕ_L and ϕ_{L_2} (0.72 ns and 4.2 ns, respectively) are difficult to assign. Visual inspection of the anisotropy decay suggests that there may be some contribution from peptide in bulk solution, similar to the 10:1 system for pure DPPC. This notion is supported by the lifetime distribution analysis, which displayed shifts towards values closer to those determined for free MK14- A430 in HEPES solution. Therefore, it is possible that the values of ϕ_L and ϕ_{L2} correspond to the same terms for free MK14-A430 but are shortened due to coupling of depolarisation times (equation (5)). To test this, a global analysis was performed with the three systems that appeared to display contributions of free peptide: free MK14-A430 and L:P = 10:1 for both pure DPPC and DPPC-Chol. The three correlation times were linked as global fit parameters. This returned reasonable fits for all three decays, with $\phi_s = 0.16$ ns, $\phi_L = 1.5$ ns and $\phi_{L2} = 10$ ns. These correlation times are very similar to those of free MK14-A430, suggesting a contribution of free peptide for the two SUV systems at L:P = 10:1.

Therefore, it appears that both the pure DPPC and DPPC-Chol SUV systems are saturated with peptide between L:P = 20:1 and 10:1. This result is interesting, as it suggests that despite the different peptide location within the bilayer, the apparent binding of the peptide to both lipid systems is similar. This is in contrast to previous studies which have described decreased binding of similar peptides to cholesterol-containing bilayers [44, 53].

Another interesting observation is that both SUV systems' fluorescence anisotropy decays do not appear to change significantly with L:P, aside from where free peptide is apparent. Other studies performed by our research group suggested transmembrane pore formation of MK14-A430 with both pure DPPC SUVs [52] and GUVs [50]. It is possible that the fluorescence lifetime and anisotropy data indicate that A430 still sampled the lipid headgroup region in a pore-forming state. This was suggested from earlier published studies within this work [29] and presented as evidence of toroidal pore formation.

3.1.10 Evanescent wave-induced time-resolved anisotropy measurements

The use of EW-excitation for TRAMs measurements [30, 80, 81] (EW-TRAMs) allows temporal resolution and separation of fluorescence depolarisation processes parallel and perpendicular to the interfacial plane. It should be noted that due to the configuration of the EW-TRAMs setup, the lateral plane of the lipid bilayer is parallel to the plane of the SiO_2-water interface where the evanescent wave is generated. Thus, in-plane anisotropy decay refers to depolarisation processes in the lateral plane of the lipid bilayer and out-of-plane anisotropy decay refers to depolarisation processes at an angle normal to the lateral plane of the bilayer (effectively, the hemisphere that is bisected by the interfacial plane, which extends into the aqueous surrounds).

3.1.11 EW-TRAMs of Melittin P14K-A430 with DPPC supported lipid bilayers (SLBs)

The EW-TRAMs decay profiles for both in- and out-of-plane excitation of MK14-A430 in the presence of DPPC SLBs (overnight-incubated and at equilibrium) are shown in figure 6. For both systems, the fluorescence anisotropy decays with time, which indicates that the fluorophore had mobility both in and out of the plane of the SLB.

For the overnight-incubated system, the change in $r(t)$, and hence the degree of mobility, was significantly more marked in the plane of the SLB than out of the plane. The anisotropy profiles can be well fit by a number of models. Therefore, the simplest appropriate model—the single-exponential hindered-rotator (equation (2))—was first used to fit the data. It is more difficult to unambiguously fit the anisotropy data out of the SLB-plane due to the small depolarisation amplitude change. Applying a global fit with ϕ linked for the in- and out-of-plane data returned a correlation time of 2 ns, with acceptable fits for data in both planes. The limiting anisotropy values, r_0 and r_∞ were not fixed for the in- or out-of-plane data. The fit returned values of $r_0 = 0.230$ and $r_\infty = 0.131$ in the SLB-plane, with $r_0 = -0.239$ and $r_\infty = -0.219$ for the out-of-plane data. It should be noted that these values are different to the theoretical values of r_0 for EW-TRAMs experiments. The value of $r_0 = 0.38$ returned from a Perrin equation fit (data not shown) indicated very close to parallel absorption and emission transition dipole moments for this fluorophore. In this case, the values of r_0 should be close to 0.5 in the plane of the interface and -0.2 out of the plane. The value of $r_0 < -0.2$ for the out-of-plane data suggests erroneous values determined for the correction factor which, as reported previously [22], is inherently difficult to determine. The value of $r_0 < 0.5$ for the in-plane data suggests that some unresolved fast depolarisation processes may have occurred, similar to that observed for the bulk solution and SUV decays. If the restriction to motion was provided by an effective cone with hard walls (the wobbling-in-cone model) [55], the cone angles for the in-plane motions would be 34° for the observed processes ($r_0 = 0.230$ and $r_\infty = 0.131$), or 51° for all processes ($r_0 = 0.5$). For out-of-plane motion, the cone angle was determined to be 14° for the observed motions. Therefore, the mobility of A430 is geometry-dependent, with the restriction to probe motions clearly greater out of the SLB-plane than in-plane.

The findings of nonzero r_∞ values may also be due to motions that were not resolvable within the timescale of the A430 fluorescence. This is supported by attempts to

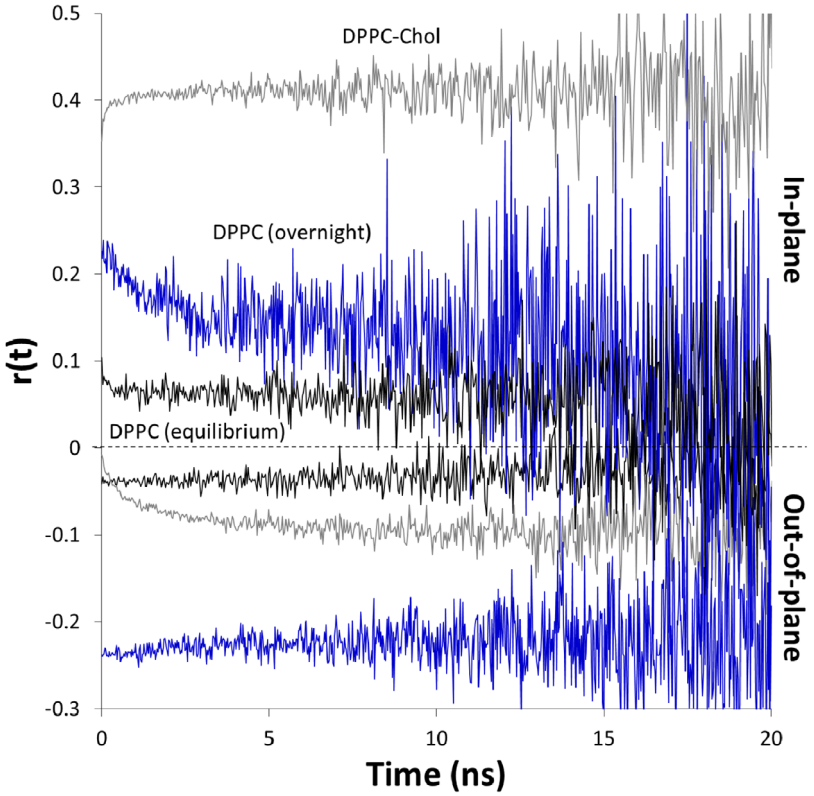

Figure 6. Fluorescence depolarisation kinetics of MK14-A430 interacting with a DPPC SLB after overnight incubation (blue curves) and at equilibrium (black curves) as well as with a DPPC-Chol SLB at equilibrium (grey curves). Data were obtained in and out of the SLB-plane using EW-TRAMs.

fit a second exponential component to the data, which resulted in acceptable fits with a broad range of values (15 ns $< \phi <$ 110 ns) for the longer correlation time. Therefore, what can be concluded from the analysis results is that A430 reported on environments of significantly different mobility (one ϕ of $\sim$2 ns and one essentially infinite on the timescales reported). These values of ϕ are similar to those reported for the SUV-peptide system. As described earlier, the value of $\phi \approx 2$ ns was attributed to A430 motions at the end of its attachment near a membrane-water interface, while the values at longer timescales (including r_∞) were attributed to peptide backbone fluctuations and rigid-body rotational diffusion. The interfacial region of lipid bilayers was described earlier as one of high motional restriction.

The EW-TRAMs decays for the DPPC SLB:MK14-A430 system at equilibrium display significant changes in A430 mobility compared to the overnight-incubated system. The initial anisotropy values were significantly lower than those for the overnight-incubated system, in both planes. This indicates a significant degree of unresolved motions at the beginning of the EW-TRAMs decay, similar to what was observed for the DPPC-Chol SUV systems. This was attributed to very fast motions that occurred during the stage of polarised fluorescence decays that were convoluted with the IRF (which was broader for the EW- compared with bulk solution measurements). If a depolarisation process of $\sim$100 ps is assumed for unhindered probe motions (as observed through the DPPC-Chol SUV measurements) then over the timeframe of the IRF, the anisotropy will decay to 14% of its original value. This corresponds to values of r(200 ps) = 0.07 in-plane and 0.03 out-of-plane, similar to the values observed here ($r_0 = 0.08$ in plane, 0.04 out of plane).

The in-plane fluorescence anisotropy decay of the equilibrium DPPC SLB system is well fit by either of the simplest applicable models: a single-exponential hindered rotator model (equation (2)) or an unhindered two-exponential model (equation (4)). The small amplitude of resolvable motions means that more than two components (i.e. one correlation time and r_∞ or two correlation times) cannot be fit unambiguously. Both models return a short correlation time in the range of 100–250 ps for processes at short timescales, supporting the idea of rapid probe motions. The longer timescale data can be well-represented by either an r_∞ value of 0.06 or a $\sim$50 ns correlation time of a similar amplitude. This indicates the presence of slow motions that cannot be accurately resolved on the timescale of A430 fluorescence.

The EW-TRAMs decay out of the SLB-plane does not show any resolvable fast motions, while a small amplitude of apparently restricted motion is observed. Attempting to fit the data with the simple expression $r_\infty = r_0$ cannot accurately model the data over the timescale of fluorescence. The data are better represented by an unhindered single-exponential model, where the correlation time of $\sim$50 ns from the in-plane result can be globally fit to both planes.

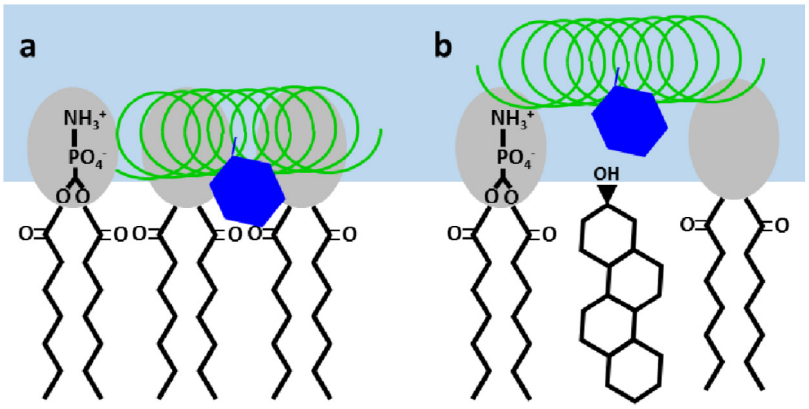

Figure 7. Schematic of the different environments experienced by the A430 probe (blue hexagon) when attached to melittin P14K (green helix) in the presence of (a) DPPC and (b) DPPC-Chol SUVs. The light blue region illustrates the aqueous solution. The probe microenvironment is a more constricted carbonyl region of the lipid bilayer for DPPC bilayers, with less water penetration. When cholesterol is present, greater lipid headgroup spacing provides more freedom for probe fluctuations as well as increased water exposure.

As described above, analysis of the in- and out-of-plane data for both the overnight-incubated and equilibrium DPPC systems show that the A430 emission depolarises via fast (100 ps to ~2 ns) and slow (>50 ns, r_∞) processes. These were attributed to probe fluctuations and a combination of peptide segmental and whole-body motions, respectively. The peptide body motions are difficult to resolve on the timescale of A430 fluorescence and thus, differences in rates of peptide motion cannot be elucidated. However, there is a clear difference in the mobility of the probe motions, both in terms of rate and freedom. The differences in the data suggest that the fast motions are from probe fluctuations within the interfacial region of the bilayer after overnight incubation, while at equilibrium the anisotropy decay is dominated by probe fluctuations in aqueous solution. The results of the TREWIFS decays appear to support this, indicating a probe environment that is more polar at equilibrium. This may indicate a change in probe location from the interfacial region ($\phi \approx 2$ ns) to the aqueous environment, with no interaction with the lipid or peptide ($\phi \approx 100$ ps). However, it should be noted that the unresolved motions for the overnight-incubated system (in-plane $\phi < 0.5$) might also represent rapid probe motions in an aqueous medium. In such a scenario, the contribution of probe motions in an aqueous environment increases from the overnight incubation to equilibrium, rather than a pure change from interfacial region to aqueous medium.

3.1.12 The influence of cholesterol

The EW-TRAMs data for the DPPC-Chol SLB system (figure 6) displayed significantly different behaviour to all other anisotropy measurements performed in this study. As was observed for the pure DPPC system, the values of r_0 were within the bounds of the theoretical values of 0.5 and −0.2 for the in- and out-of-plane data: 0.35 (in-plane) and −0.01 (out-of-plane). However, an *increase* in *r(t)* was observed with time rather than a decay. Similar time-dependent fluorescence anisotropy behaviour has been observed before in lipid bilayers [82, 83]. This behaviour has been attributed to fluorescence decay times being associated with different rotational correlation times, as a result of different environments being experienced by the fluorophore. For example, a fluorophore population with a short fluorescence lifetime that also has fast, unhindered motion, will cause a rapid decay of the fluorescence anisotropy. However, this population's contribution to the fluorescence anisotropy will decrease as its fluorescence intensity decays. If the fluorescence lifetime is significantly shorter than other species with slower or more hindered rotation, a recovery of the fluorescence anisotropy signal will be observed as a function of time. This behaviour, termed 'dip and rise', has been summarised elsewhere [84] and is typically analysed with a model that associates a particular correlation time with a fluorescence lifetime, typically of the form $r(t) = f_i(t)r_i(t) + r_\infty$, where $f_i(t)$ is the fractional contribution of component i to the overall fluorescence intensity at time t.

Unfortunately, the inability to resolve this fast depolarisation means that the application of this associative model cannot be made. However, assuming that unresolvable fast motions are responsible for lower r_0 values than expected, it can be suggested that the rate of fluorescence recovery is due to the decay of fluorescence intensity of rapidly-depolarising populations of the A430 probe. To test this theory, it is assumed that the fluorescence recovery occurs exponentially, as would the fluorescence intensity decay. In this case, an exponential fitting function can be employed to provide a quantitative estimate of the rate of fluorescence anisotropy recovery. In this analysis, reverse (i.e. negative) preexponentials were used to estimate these 'rise' times.

The EW-TRAMs profiles can be well-fit with a range of parameters for this exponential fit. A two-exponential global fit with linked rise times of 0.7 ns and 3.7 ns (τ_1 and τ_3 fluorescence lifetime components,

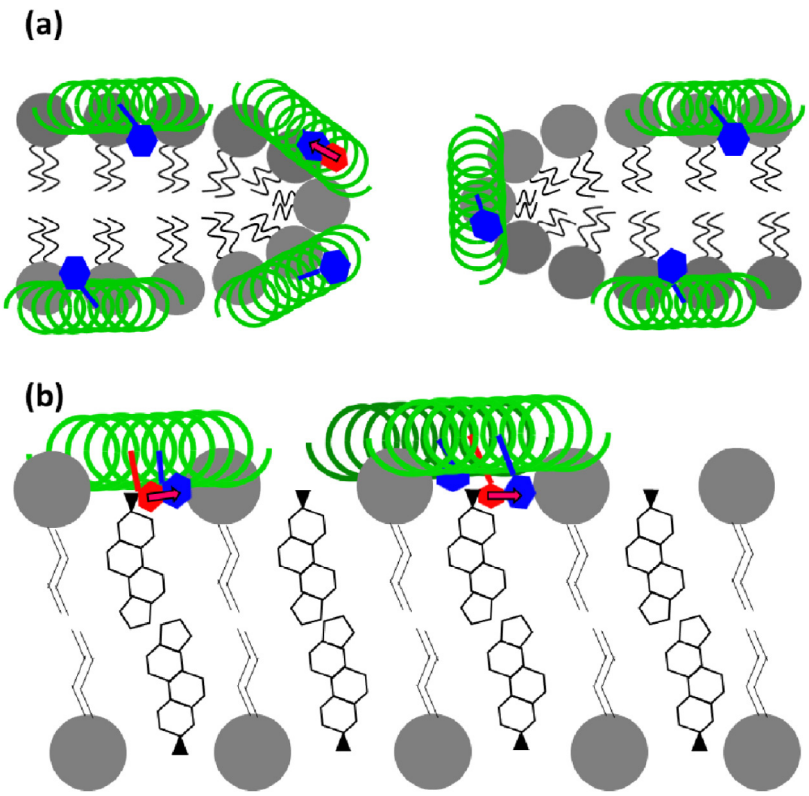

Figure 8. Schematic illustrating the suggested peptide-probe configurations in (a) DPPC and (b) DPPC-Chol SLBs. MK14-A430 forms a large number of pores in DPPC SLBs, with A430 appearing to locate near the headgroup-water interface. A small degree of hindered motion arises from a more deeply embedded population of A430. All of the A430 population appears to locate near the headgroup-water interface of DPPC-Chol bilayers, with a large amount of free A430 motions. However, there is a population with greatly restricted mobility, which appears to be in close proximity with neighbouring indole electron donors (red hexagons, with electron donation depicted by pink arrows). Note that a small degree of transmembrane pore formation is suggested by the data but is not shown in (b).

table 5) for the in- and out-of-plane EW-TRAMs decays models the data well, except at very short timescales (<100 ps) where the IRF will still be convoluted with the decays. For the in-plane profile, the fit returned no 3.7 ns component. This is likely due to the small rise in amplitude, making resolution of any longer timescale components difficult. The fact that the fluorescence lifetime components can be well fit to the data suggests that any resolvable motions of A430 were either slow compared to the fluorescence lifetimes or greatly restricted. This is supported by the results of the global fit, which returned r_∞ values of 0.41 (in-plane) and −0.10 (out-of-plane). No resolvable decay component is apparent at longer t, after the rise component of the anisotropy profile. This, combined with the r_∞ values, indicate a probe population with significant restriction to motion in both planes. Analysis using the wobbling-in-cone model returned cone-angles of 21° in-plane and 38° out-of-plane.

Inclusion of the 1.8 ns fluorescence decay component in the analysis of EW- TRAMs rise behaviour could not provide an acceptable fit. This suggests that this component was not involved in the rapid decay of the fluorescence anisotropy, or had significantly restricted motion. This lifetime was close to that found for the quenched lifetime of the pure DPPC SUVs, suggesting that the 1.8 ns lifetime is due to a population of A430 that has penetrated the bilayer interfacial region. The high motional restriction of this region could explain the high r_∞ values. Interestingly, despite low apparent mobility, there is a high extent of quenching for this population of probes. This indicates a high local population, but might also be due to the aromatic structure of indole in tryptophan. Aromatic amines have been found to have nominal orientation requirements to engage in PET with coumarin molecules [35]. Another possibility is that the PET donor-acceptor pair is well-aligned within this matrix, within these motional constraints.

3.2. Discussion

By monitoring the fluorescence of A430 when attached to melittin P14K, the location and dynamics of the peptide in lipid environments have been investigated. A number of peptide environments and arrangements have been suggested from these fluorescence studies. Therefore, it appears most convenient to interpret the data with respect to the existing models for lytic peptide behaviour: the carpet, barrel-stave and toroidal pore models. Briefly, the carpet model suggests that peptides reside at the membrane-water interface, with the long axis of the helix aligned parallel to the membrane surface (S-state) and the hydrophobic face facing the membrane. The pore models describe the long axis of

the peptide helices aligned with the long axis of the helix traversing the lipid bilayer (I-state). The barrel-stave model describes an oligomeric pore structure, with the hydrophobic face of the helices facing the acyl chains of the lipid bilayer and the hydrophilic faces lining the pore interior. In the toroidal pore model, lipids bend through to line the pore surface along with the hydrophilic faces of the peptides.

Time-resolved fluorescence studies with the DPPC SUVs showed that the peptide located near the carbonyl moiety within the interfacial region of the lipid bilayer (figure 7). The addition of cholesterol resulted in a decrease in probe penetration into the bilayer, appearing to locate near the lipid headgroups. This shallower location of the probe resulted in greater fluorescence quenching by PET. For both DPPC and DPPC- Chol SUVs, no conclusive evidence of transmembrane (I-state) peptide could be determined. Indeed, the TRAMs measurements suggested that a contribution from free peptide was responsible for the change in fluorescence behaviour at low L:P. Therefore, it is suggested that in the SUV systems, the peptide behaves according to the carpet model under the conditions studied.

The TREWIFS data for MK14-A430 after overnight incubation with a DPPC SLB showed a probe environment of moderate polarity, indicating a location near the lipid headgroups. A similar but more polar environment was experienced after the system had reached equilibrium. This was supported by the EW-TRAMs data, which showed a greater contribution of a more rapidly-diffusing pore population at equilibrium. These changes were suggested to be a result of increased pore formation with incubation time, with both systems involving a combined S- and I- state peptide arrangement. This is supported by the fluorescence lifetime distribution analysis for the equilibrium system, which suggested that there may be two probe populations corresponding to different peptide arrangements. A combined surface/transmembrane pore model appears to best describe the behaviour of MK14-A430 when associated with DPPC SLBs.

As for the pore-forming behaviour, the lipid headgroup location (as indicated from the A430 fluorescence) suggests that the toroidal pore model provides the most accurate representation (figure 8). If the barrel-stave model represented pore formation, the A430 probe at the K14 position would either have access to the acyl chain region of the SLB (very non-polar) or the aqueous interior of the pore. Both of these locations would involve the considerable motional freedom observed in the equilibrium scenario. However, the shallow headgroup location (suggested from the discrete analysis of the TREWIFS data) was also shown to have considerable freedom from the TRAMs studies on DPPC-Chol SUV systems. Therefore, it is believed that the behaviour of MK14-A430 associated with DPPC SLBs is best described by a mixed carpet/toroidal pore model.

In the DPPC-Chol SLB, A430 appears confined within an environment of similar polarity to the lipid interfacial region (both quenched and unquenched species). There is a body of evidence to suggest that MK14-A430 undertakes an S-state arrangement when associated with the DPPC-Chol SLB. Analysis of the fluorescence decay kinetics suggests a very similar environment to the DPPC-Chol SUVs (figure 3), for which there was no evidence of I-state peptides. The only significant difference between the systems is the greater quenching in the SLB. This may be explained by the lower L:P in the SLB systems (estimated to be ~2:1 for a single SLB in the TREWIFS cell) and suggests a high local concentration in a like arrangement. The EW-TRAMs data showed significant motional restriction in both planes of the SLB for a population of the probe, particularly parallel to the bilayer surface. This may also support the notion of S-state peptide, where the probe may be interdigitated between the lipid headgroups. This arrangement would suggest that motions in the lateral plane of the SLB would be more greatly hindered than those perpendicular to the SLB surface, as is observed.

How, then, can these results be reconciled? It is possible that the ratio of S-state to I-state MK14-A430 is significantly greater with the DPPC-Chol SLB compared with the DPPC SLB. This could explain why data suggesting S-state peptide dominates the results from the experiments described above. Previous studies have shown that cholesterol inhibits the ability of native melittin to insert in a transmembrane fashion [53]. Therefore, it appears that a mixed carpet/toroidal pore model may also account for the behaviour displayed with DPPC-Chol, with a lower extent of pore formation and shallower penetration depth of peptides in the S-state.

The interesting behaviour observed by EW-TRAMs for the DPPC-Chol SLB system might be explained by the entire A430 population being confined in the proximity of the lipid headgroups. The high extent of quenching suggests a high local concentration of peptide in a similar environment, which could be explained by a predominantly surface state. Probe molecules in aqueous solution near the headgroup surface would diffuse freely which could explain the rapid depolarisation. Also, it is possible that the lower hydration of the L_0-phase DPPC-Chol than the S_0-phase DPPC will result in the decreased mobility observed for the probe population that has penetrated the headgroup region.

Acknowledgments

The authors acknowledge the support by the International Research and Research Training Fund (IRRTF) from the University of Melbourne.

References

[1] Spratt B G and Cromie K D 1988 *Rev. Infect. Dis.* **10** 699–711
[2] Chopra I 1985 Mode of action of the tetracyclines and the nature of bacterial resistance to them *The Tetracyclines. Handbook of Experimental Pharmacology* vol 78, ed J Hlavka and J Boothe (Berlin: Springer) pp 317–92
[3] Brisson-Noël A, Trieu-Cuot P and Courvalin P 1988 *J. Antimicrob. Chemother.* **22** (Suppl B) 13–23
[4] Fourmy D, Recht M I, Blanchard S C and Puglisi J D 1996 *Science* **274** 1367–71
[5] Wolfson J S and Hooper D C 1989 *Clin. Microbiol. Rev.* **2** 378–424
[6] Walsh C 2000 *Nature* **406** 775–81
[7] Cowan M M 1999 *Clin. Microbiol. Rev.* **12** 564–82
[8] Hancock R E W and Sahl H G 2006 *Nat. Biotechnol.* **24** 1551–7
[9] Habermann E 1972 *Science* **177** 314–22
[10] Zasloff M 1987 *Proc. Natl Acad. Sci. USA* **84** 5449–53
[11] Kokryakov V N, Harwig S S, Panyutich E A, Shevchenko A A, Aleshina G M, Shamova O V, Korneva H A and Lehrer R I 1993 *FEBS Lett.* **327** 231–6
[12] Steiner H, Hultmark D, Engström Å, Bennich H and Boman H G 1981 *Nature* **292** 246–8
[13] Meyer C E and Reusser F 1967 *Experientia* **23** 85–6
[14] Wilbrandt W 1948 *Pflugers Arch. Gesamte Physiol. Menschen Tiere* **250** 569–76
[15] Habermann E 1954 *Naunyn. Schmiedebergs. Arch. Exp. Pathol. Pharmakol.* **222** 173–5
[16] Habermann E and Jentsch J 1967 *Hoppe. Seylers. Z. Physiol. Chem.* **348** 37–50
[17] Dempsey C E 1990 *Biochim. Biophys. Acta* **1031** 143–61
[18] Raghuraman H and Chattopadhyay A 2007 *Biosci. Rep.* **27** 189–223
[19] Fennell J F, Shipman W H and Cole L 1968 *J. Exp. Biol. Med.* **127** 707–10
[20] Lubke L L and Garon C F 1997 *Clin. Infect. Dis.* **25** S48–51
[21] Wachinger M, Kleinschmidt A, Winder D, Pechmann N V, Ludvigsen A, Neumann M, Holle R, Salmons B, Erfle V and Brack-Werner R 1998 *J. Gen. Virol.* **79** 731–40
[22] Smith T A, Gee M L and Scholes C A 2005 Time-resolved evanescent wave-induced fluorescence anisotropy measurements *Reviews in Fluorescence* ed C Geddes and J Lakowicz (Berlin: Springer) pp 245–70
[23] Crystall B, Rumbles G, Smith T A and Phillips D 1993 *J. Colloid Interface Sci.* **155** 247–50
[24] Rumbles G, Brown A J and Phillips D 1991 *J. Chem. Soc. Faraday Trans.* **87** 825–30
[25] Sabnis R W 2015 *Handbook of Fluorescent Dyes and Probes* 1st edn (New Jersey: Wiley)
[26] Gee M L 1987 Surface forces in thin liquid films on quartz *PhD Thesis* School of Chemistry, University of Melbourne
[27] Lee M, Kim J, Tang J and Hochstrasser R M 2002 *Chem. Phys. Lett.* **359** 412–9
[28] Jensen K J 2013 Solid-phase peptide synthesis: an introduction *Peptide Synthesis and Applications* ed K Jensen and P T S Pedersen (New York: Humana Press) pp 1–21
[29] Rapson A C, Hossain J D W A, Nice E C, Clayton A H A, Smith T A and Gee M L 2011 *Biophys. J.* **100** 1353–61
[30] Gee M L, Lensun L, Smith T A and Scholes C A 2004 *Eur. Biophys. J.* **33** 130–9
[31] O'Connor D V and Phillips D 1984 *Time-correlated Single Photon Counting* (London: Academic)
[32] Löffler G, Schreiber H and Steinhauser O 1997 *J. Mol. Biol.* **270** 520–34
[33] Clayton A H A, Ghiggino K P, Lawson J M and Paddon-Row M N 1994 *J. Photochem. Photobiol. A: Chem.* **80** 323–31
[34] Doose S, Neuweiler H and Sauer M 2009 *ChemPhysChem* **10** 1389–98
[35] Nad S and Pal H J 2002 *J. Chem. Phys.* **116** 1658–70
[36] Aigner D, Freunberger S A, Wilkening M, Saf R, Borisov S M and Klimant I 2014 *Anal. Chem.* **86** 9293–300
[37] Marmé N, Knemeyer J P, Sauer M and Wolfrum J 2003 *Bioconjug. Chem.* **14** 1133–9
[38] Matsuzaki K 1999 *Biochim. Biophys. Acta—Biomembr.* **1462** 1–10
[39] Shai Y 1999 *Biochim. Biophys. Acta—Biomembr.* **1462** 55–70
[40] Yang L, Weiss T M, Lehrer R I and Huang H W 2000 *Biophys. J.* **79** 2002–9
[41] De Planque M R R, Bonev B B, Demmers J A A, Greathouse D V, Koeppe R E, Separovic F, Watts A and Killian J A 2003 *Biochemistry* **42** 5341–8
[42] Kachel K, Asuncion-Punzalan E and London E 1995 *Biochemistry* **34** 15475–9
[43] Schiffer M, Chang C H and Stevens F 1992 *J. Protein Eng.* **5** 213–4
[44] Raghuraman H and Chattopadhyay A 2004 *Biophys. J.* **87** 2419–32
[45] Raghuraman H and Chattopadhyay A 2007 *Biophys. J.* **92** 1271–83
[46] Lewis F D and Letsinger R L 1998 *J. Biol. Inorg. Chem.* **3** 215–21
[47] Strauch S, Strauch S, McLendon G, McLendon G, McGuire M, McGuire M, Guarr T and Guarr T 1983 *J. Phys. Chem.* **87** 3579–81
[48] Hush N S, Paddon-Row M N, Cotsaris E, Oevering H, Verhoeven J W and Heppener M 1985 *Chem. Phys. Lett.* **117** 8–11
[49] Sisido M, Hoshino S, Kusano H, Kuragaki M, Makino M, Sasaki H, Smith T A and Ghiggino K P 2001 *J. Phys. Chem.* B **105** 10407–15
[50] Burton M G, Huang Q M, Hossain M A, Wade J D, Clayton A H A and Gee M L 2013 *Langmuir* **29** 14613–21
[51] Chen F Y, Lee M T and Huang H W 2002 *Biophys. J.* **82** 908–14
[52] Ningsih Z, Hossain M A, Wade J D, Clayton A H A and Gee M L 2012 *Langmuir* **28** 2217–24
[53] Chen L Y, Cheng C W, Lin J J and Chen W Y 2007 *Anal. Biochem.* **367** 49–55
[54] Kinosita K Jr, Kawato S and Ikegami A 1977 *Biophys. J.* **20** 289–305
[55] Kinosita K, Ikegami A and Kawato S 1982 *Biophys. J.* **37** 461–4
[56] Szabo A 1984 *J. Chem. Phys.* **81** 150–67
[57] Vogel H, Nilsson L, Rigler R, Voges K P and Jung G 1988 *Proc. Natl Acad. Sci. USA* **85** 5067–71
[58] Lakowicz J R 2006 *Principles of Fluorescence Spectroscopy* 3rd edn (New York: Springer)
[59] John E and Jähnig F 1988 *Biophys. J.* **54** 817–27
[60] Lakowicz J R, Gryczynski I, Cherek H and Laczko G 1991 *Biophys. Chem.* **39** 241–51
[61] Hu Y, Chin T M, Fleming G R and Yang N C C 1993 *J. Phys. Chem.* **97** 13330–4
[62] Georghiou S, Thompson M and Mukhopadhyay A K 1981 *Biochim. Biophys. Acta—Biomembr.* **642** 429–32
[63] Lakowicz J R, Maliwal B, Cherek H and Balter A 1983 *Biochemistry* **22** 1741–52
[64] Rex S 2000 *Biophys. Chem.* **85** 209–28
[65] Taylor J W and Kaiser E T 1987 *Methods Enzymol.* **154** 473–98
[66] Eimer W and Pecora R 1991 *J. Chem. Phys.* **94** 2324–9
[67] Tirado M M and García De La Torre J 1979 *J. Chem. Phys.* **71** 2581–7
[68] Tirado M M and García De La Torre J 1980 *J. Chem. Phys.* **73** 1986–93
[69] Tirado M M, Martínez C L and García De La Torre J 1984 *J. Chem. Phys.* **81** 2047–52
[70] Garcia de la Torre J, Lopez Martinez M C and Mercedes Tirado M 1984 *Biopolymers* **23** 611–5
[71] Porter E A, Weisblum B and Gellman S H 2002 *J. Am. Chem. Soc.* **124** 7324–30
[72] Li C and Salditt T 2006 *Biophys. J.* **91** 3285–300
[73] Yang L, Harroun T A, Weiss T M, Ding L and Huang H W 2001 *Biophys. J.* **81** 1475–85
[74] Clayton A H A and Sawyer W H 2000 *Biophys. J.* **79** 1066–73
[75] Peters R and Cherry R J 1982 *Proc. Natl Acad. Sci. USA* **79** 4317–21
[76] Aisenbrey C and Bechinger B 2004 *J. Am. Chem. Soc.* **126** 16676–83
[77] Döring K, Beck W, Konermann L and Jähnig F 1997 *Biophys. J.* **72** 326–34

[78] Maliwal B P, Hermetter A and Lakowicz J R 1986 *Biochim. Biophys. Acta—Protein Struct. Mol. Enzymol.* **873** 173–81
[79] Dornmair K and Jähnig F 1989 *Proc. Natl Acad. Sci. USA* **86** 9827–31
[80] Lensun L, Smith T A and Gee M L 2002 *Langmuir* **18** 9924–31
[81] Smith T A, Scholes C A and Gee M L 2007 Time-resolved evanescent wave-induced fluorescence studies of macromolecular adsorption *Complex Light and Optical Forces* (*Proc. of SPIE* vol 6483) ed D Andrews *et al* (Bellingham, WA: SPIE) pp 64830C1–9
[82] Wolber P K and Hudson B S 1981 *Biochemistry* **20** 2800–10
[83] Wolber P K and Hudson B S 1982 *Biochemistry* **37** 253–62
[84] Smith T A and Ghiggino K P 2015 *Methods Appl. Fluoresc.* **3** 022001